Structure and stability of ultrathin Fe films on W(110)

B. Santos
Instituto de Química-Física Rocasolano, CSIC, Madrid 28006, Spain and European Quality Assurance Spain, S.L. Madrid 28023, Spain

M. Rybicki and I. Zasada*
Solid State Physics Department, University of Lodz, ul. Pomorska 149/153, Lodz, Poland

E. Starodub and K. F. McCarty
Sandia National Laboratories, Livermore, California 94550, USA

J. I. Cerda and J. M. Puerta
Instituto de Ciencia de Materiales de Madrid, CSIC, Madrid 28049, Spain

J. de la Figuera
Instituto de Química-Física Rocasolano, CSIC, Madrid 28006, Spain
(Received 19 March 2014; revised manuscript received 11 February 2016; published 17 May 2016)

The growth of one and two atomic layers of iron on a W(110) substrate was followed by low-energy electron microscopy. The near-surface structural properties of the perfectly flat pseudomorphic films were studied by quantitative low-energy electron diffraction analysis from areas of uniform thickness as well as by the density functional theory. A strong relaxation of the outermost atomic layers was found in Fe mono- and bilayers on W(110). By calculating the phonon dispersion relations and phonon density of states, the stability of the pseudomorphic iron bilayer on a tungsten substrate has been addressed. To complete the physical picture, an iron trilayer has also been analyzed in order to identify the source of instability for its pseudomorphic phase. Our results show that the surface instability originates from the softening of the in-plane surface modes along the $[1\bar{1}0]$ direction, although the soft modes were not observed. The enhanced magnetic moments calculated within the density functional theory are in good agreement with experimental findings reported for these systems.

DOI: 10.1103/PhysRevB.93.195423

I. INTRODUCTION

The properties of epitaxial films on substrates are intimately connected to the structural mismatch between the constituent materials. Differences in the lattice parameters and/or symmetry generate interlayer strains that usually lead to surface relaxations, in-plane reconstructions, and/or promote three-dimensional growth. Fe(110) epitaxial films on W(110) are prototype systems for studying the dependence of the structural, electronic, and magnetic properties on the growth mode, film thickness, and temperature. In this system the experimentally observed lattice misfit amounts to -9.4%, which should considerably influence fundamental properties such as lattice dynamics [1], electronic [2] and magnetic structure [3], or chemical reactivity [4]. Starting from the pseudomorphic Fe monolayer on W(110) [5], through ultrathin films [5,6] to thicker Fe(110) films that mimic the surface properties of bulk Fe [7], this system is one of the most intensely investigated in surface science. In particular, the growth of Fe/W(110) has been investigated by low-energy electron diffraction (LEED), Auger electron spectroscopy [1], scanning tunneling microscopy (STM) [6,8,9], and surface x-ray diffraction [10].

The growth takes place pseudomorphically for the first monolayer (1 ML) despite the large lattice misfit between the bulk phases of both elements ($a_W = 3.16$ Å and $a_{Fe} = 2.86$ Å). The growth after the first monolayer depends strongly on the particular conditions employed, such as temperature, flux, and cleanliness of the substrate. The second layer grows pseudomorphically up to some coverage (the well-known "sesquilayer" film [9]), and dislocations that relax the lattice mismatch between film and substrate have been reported to develop already before a complete 2 ML film can be grown [5,6]. Films thicker than 2 ML are not pseudomorphic and contain a network of misfit dislocations that can be observed in STM images [6] and by the presence of satellite spots in the LEED pattern [5]. Thicker films of Fe(110) on W(110) in the 25–200 Å range reproduce the Fe bulk surface properties [11]. Since the in-plane lattice spacing of the Fe monolayer and bilayer are expanded compared to bulk Fe, reduced interlayer spacings relative to the bulk W value [12] are expected. This effect has been observed in similar systems such as Cr/W(110) [13] or Ni/W(110) [14], and has been reported for Fe films of mixed thickness on W(110) [10].

Magnetically, Fe/W(110) is one of two systems known to date whose spin changes orientation with each additional atomic layer of film (the other system with successive spin-reorientation transitions is Co/Ru [15]): while 1 ML has an in-plane magnetization with a Curie temperature below RT, pseudomorphic bilayer islands above a critical size present out-of-plane magnetization. Thicker films and islands present again an in-plane magnetization [5]. Recent results by nuclear resonant scattering further revealed the complex character of this transition and showed a strong enhancement of the surface magnetic moment that amounts to more than 25% [16]. The

*izasada@wfis.uni.lodz.pl

study of the magnetic properties is further complicated by the extreme sensitivity of the system to hydrogen adsorption, which changes the easy axis of bilayer islands [17].

The magnetic and structural properties of pseudomorphic iron on a tungsten substrate have also been studied theoretically within the density functional generalized gradient approximation (DFT-GGA) [18]. By studying the spectrum of surface phonons, a strong dependence of the lattice dynamics on the magnetic interactions has been revealed. The ferromagnetic ordering has been found crucial in stabilizing the Fe monolayer on W(110) [18].

In the present work we focus on the crystallographic structure and stability of Fe mono- and bilayer films on the W(110) surface using low-energy electron microscopy (LEEM) [19,20], LEED, and DFT calculations. LEEM allows monitoring film growth in real time, which greatly facilitates finding the growth conditions that provide flat, uniformly thick, pseudomorphic layers. We determine the surface structure by analyzing how the intensity of diffraction spots changes with electron energy, i.e., LEED-$I(V)$. A unique feature of this study is that we analyze the structure of film areas known to contain exactly 1 or 2 ML Fe. In particular, this study represents a structural determination of micrometer-sized bilayer Fe/W islands. Our study confirms a noticeable variation of the atomic interlayer spacing in the Fe(110) bilayer and also demonstrates that epitaxial strains are present in the film. The structural results of LEED are confirmed by DFT-based total energy calculations. Moreover, since the DFT approach enables an efficient description of lattice dynamics in surface systems [21], we have additionally performed first-principles calculations of the phonon excitation spectrum [22] for iron mono-, bi- and trilayer films on the W(110) surface in order to analyze their stability. We address the last system to consider the possibility of growing thicker pseudomorphic Fe layers on W(110). For completeness, we calculated the layer-resolved magnetic moments in all three systems.

The outline of the paper is as follows. The experimental details are described in Sec. II. Section III is devoted to the structure determination. In Sec. III A we discuss LEEM/LEED results and their quantitative analysis, while in Sec. III B the DFT calculations are presented together with the phonon spectra. Finally, in Sec. IV we compare our results with other studies of ultrathin Fe films as well as thicker Fe films grown on W(110) surface and present a summary and the conclusions of this work.

II. EXPERIMENTAL DETAILS

A commercial Elmitec LEEM was used to characterize both the growth and the crystal structure of 1 and 2 ML of Fe on W(110). The film growth was followed in real time while Fe was dosed on W(110).

Iron was evaporated by electron bombardment at a typical flux of 0.2 AL min^{-1} while keeping the substrate temperature at 550 K. During the experiments, the background pressure in the experimental chamber remained in the 10^{-10} mbar range. The W(110) crystal was cleaned by exposure to O_2 followed by repeated flashes to 2200 K in order to remove any residual oxygen on the surface. The cleanliness of the crystal was checked by LEEM and LEED. The LEED pattern acquired from the W(110) crystal always showed a sharp (1×1) pattern prior to the Fe deposition. The $I(V)$ curves are acquired within the LEEM instrument by changing the power of the lenses in order to image the back-focal plane of the objective lens. Using LEEM as a LEED diffractometer [13,20] has several advantages over a conventional LEED system: the specular beam can be acquired in normal incidence and diffraction from a single substrate terrace or film island can be measured. Also, the data can be acquired at elevated temperatures. The LEED-$I(V)$ data was obtained on perfect 1 and 2 ML Fe films on W(110) from 0.5-μm-diameter areas on a single film island using an illumination aperture to limit the size of the electron beam on the sample. The curves were acquired at 550 K sweeping a 30–350 eV energy range. The (00), four symmetry-equivalent (01) and two symmetry-equivalent (11) beams were measured, giving a total energy range $\Delta E =$ 900 eV. The Pendry R factor R_p [23] between equivalent beams was always lower than 0.20, thus ensuring that normal incidence was achieved with good precision.

III. STRUCTURE DETERMINATION

A. LEEM and LEED

The growth of Fe on W(110) has been performed by many groups [6,10,24,25]. From these studies it is clear that while the first layer is pseudomorphic when grown on the substrate at room temperature or hotter, three layers or thicker always present a misfit dislocation network to adapt the lattice mismatch between Fe and W. The transition regime from pseudomorphic to a relaxed film occurs through the nucleation and growth of misfit dislocations within a film thickness of 2 ML. For example, by time-lapsed STM [24] the formation of the dislocations was detected on 2 ML islands larger than 9 nm in width, while by real-time surface x-ray diffraction, already relaxed 2 ML islands with coverages as low as 1.2 ML [10] were observed. Both mentioned experiments were carried out at room temperature. Using a higher substrate temperature, several groups [24,25] obtained films of mostly pseudomorphic 2 ML with just a few isolated dislocation lines. It is clear from the published experiments that the bilayer is at the very limit of the pseudomorphic stability, and that particular details of a given sample and growth conditions can trigger the nucleation of the misfit dislocations at different 2 ML coverages: terrace size, impurities, temperature, etc. This is consistent with the nucleation of dislocations in other systems close to the stability limit. For example, misfit dislocations can be nucleated on films 1 ML Cu [26] or Co on Ru(0001) [27] by supersaturating the surface with adatoms, and their climb and glide has been observed at room temperature [28,29]. Often, the nucleation of misfit dislocations originates at nuclei of (dislocated) thicker islands [2 ML for Cu on Ru, or 3 ML for Fe on W(110)], overcoming in this way the kinetic barrier for dislocation nucleation.

1. Pseudomorphic growth

In our case, we follow in real time the growth front by LEEM. We selected relatively large terraces (to prevent step-induced multilayer growth [27]), and a temperature high enough to easily observe the islands of each level. Figure 1

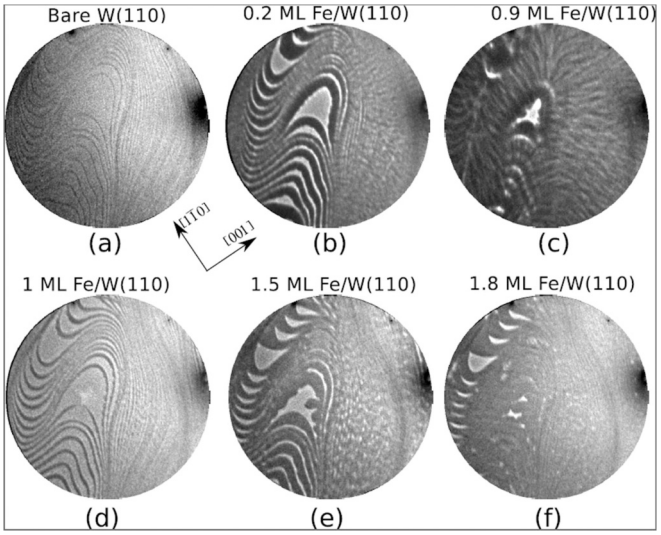

FIG. 1. LEEM images acquired during the deposition of 2 ML of Fe on W(110). The growth takes place layer by layer in the step-flow mode. (a) Image of the bare W(110) surface prior to the Fe deposition, (b)–(d) completion of the first layer, and (e), (f) images acquired during the growth of the second layer of Fe. The temperature of the substrate is 550 K, the field of view is 7 μm, and the electron beam energy is 5.5 eV.

shows a sequence of images acquired during the deposition of close to 2 ML Fe on W(110). The bare W(110) surface prior to the Fe deposition is shown in Fig. 1(a). Different terraces separated by monoatomic steps (thin gray lines) can be observed on the bare surface of W(110). Fe grows initially by nucleating at the substrate step edges forming ribbons, and in very large terraces (not shown) also by nucleating islands in the middle. The edges of the 1 ML bands become undulated as they advance from the W steps. This suggests that the 1 ML front is morphologically unstable during growth. At 5.5 eV electron energy, the Fe film appears darker than the substrate, as shown in Fig. 1(b). As further Fe is deposited, the first Fe layer is completed by a nearly perfect step flow [Figs. 1(c) and 1(d)]. Unlike growth at lower temperature [10,24], the second Fe layer starts to grow only when the first layer is completed [6], as shown in Fig. 1(d). The second layer growth begins also from the substrate steps and it proceeds until the terrace is almost filled up. If the growth is continued above the 2 ML limit into the nucleation of 3 ML islands, the quasi-step flow breaks down, and thicker layers nucleate on top of each other (not shown).

To study the structure of the films selected area LEED and LEED-$I(V)$ are used. Figures 2(a) and 3(a) show selected-area LEED patterns acquired on uniformly 1- and 2-ML-thick Fe regions, respectively. The (1 × 1) integer spots are in the same positions as the substrate spots in both cases, indicating that both 1 and 2 ML of Fe/W(110) grow in a pseudomorphic manner with the substrate. The slight asymmetries in the LEED spots arise from small misalignments in the electron lens. The temperature is high enough that dislocations in the film should be quite mobile [26], so if present, they would be expected to order and give a LEED pattern, in a similar way to the one observed for dislocations in 1 ML Cu/Ru(0001) [30]. There is no hint whatsoever of additional spots in the LEED patterns

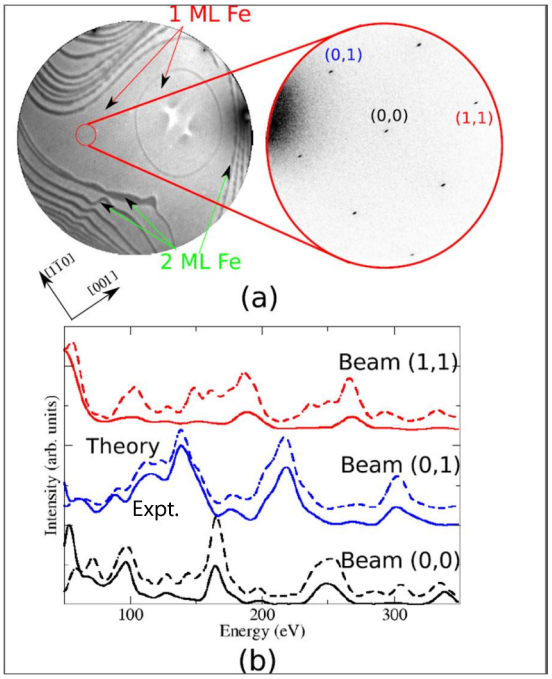

FIG. 2. (a) LEEM image acquired after the deposition of a 1 ML Fe/W(110). The field of view was 7 μm and the electron beam energy was 5.5 eV. LEED pattern (150 eV) obtained from a 1 ML Fe area on a single W(110) terrace. The (1 × 1) pattern shows that the film is pseudomorphic. (b) LEED-$I(V)$ data (solid lines) and best fit $I(V)$ curves (dashed lines) for different beams.

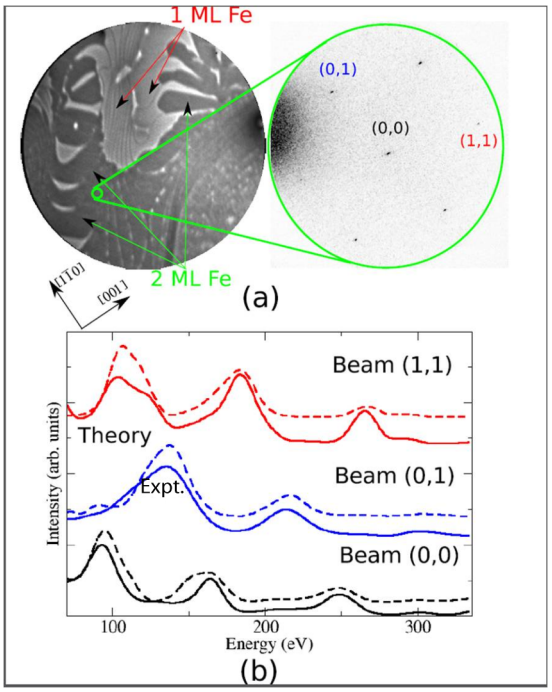

FIG. 3. (a) LEEM image acquired after the deposition of a 2 ML Fe/W(110). The field of view was 7 μm and the electron beam energy was 5.5 eV. LEED pattern (150 eV) obtained from a 2 ML Fe area on a single W(110) terrace. The (1 × 1) pattern shows that the 2 ML film is pseudomorphic. (b) LEED-$I(V)$ data (solid lines) and best fit $I(V)$ curves (dashed lines) for different beams.

[see Figs. 2(a) and 3(a)]. Although we cannot exclude the presence of a few disperse dislocation lines so far away and/or disordered as to render them undetectable by LEED, we note that also we do not observe any sign of dislocations in real-space LEEM, while dislocations close to the surface are usually easily detectable in LEEM mode due to phase contrast [20]. In contrast, even a small amount of 3 ML Fe/W(110) provides a LEED pattern typical of a dense network of misfit dislocations. In consequence, we suggest that, under our growth conditions and at 550 K, the 2-ML-thick Fe films of micrometer size are stable on W(110).

2. *LEED calculations*

To obtain the interlayer spacings of the films, LEED-$I(V)$ fits were carried out [see Figs. 2(b) and 3(b)]. Fully dynamical LEED-$I(V)$ curve calculations were performed with a modified version of the Van Hove–Tong package [31,32]. The surface was modeled by stacking one or two monolayers of Fe on top of five layers of W(110) bulk, respectively, using the renormalized forward scattering approach. Relativistic phase shifts were calculated and subsequently spin averaged [33]. We explored the parameter space comprised of the topmost three interlayer spacings by calculating the $I(V)$ curves over fine three-dimensional (3D) parameter grids. The interlayer spacings were swept over wide ranges. The experiment-theory agreement was quantified via Pendry's R factor R_p [23], while the error bar for each parameter was obtained from its variance $\mathrm{Var}(R_p) = R_{p\,\min}\sqrt{(8V_{0i}/\Delta E}$, where V_{0i} gives the imaginary part of the inner potential. Correlations between the structural parameters were taken into account for the estimation of the error limits. We note that all structural parameters derived in this work represent well-defined minima in their respective R-factor plots. Other nonstructural parameters such as the muffin-tin radius, the inner potential, or the Debye temperatures at the surface planes were also optimized. The structural parameters obtained in the best LEED-$I(V)$ fits are shown in Table I.

For the case of 1 ML Fe/W(110), the best fit ($R_p = 0.14$) yields a large contraction of -10.3% for the topmost Fe layer towards the W(110), in very good agreement with both theoretical and experimental results reported previously [10,34–36]. One can also notice that the first and second W(110) layers do not present any significant changes in their interlayer spacings with respect to the bulk W value of 2.24 Å.

For the case of 2 ML Fe/W(110), the best LEED-$I(V)$ fit ($R_p = 0.16$) leads to an even larger contraction of -16.6% between the two Fe layers, d_{12}. This large contraction has been reported in mixed 1–3 ML films by x-ray diffraction [10] as well as predicted theoretically [37,38]. On the other hand, the LEED-$I(V)$ fits yield that the interlayer spacing for the first Fe layer above the W is equal to 2.00 Å, similar to d_{12} in the 1 ML case.

B. DFT and phonon dispersion curves

The DFT calculations were performed in a slab geometry using the Perdew-Burke-Ernzerhof generalized gradient approximation functional [39] implemented in the VASP program [40]. Symmetric slabs along the W-bcc (110) direction were built within the C_{mmm} symmetry constraints of the space group. Calculations performed for clean tungsten slabs showed that the interlayer distance between the central layers converged slowly with increasing slab thickness, and that at least seven layers were required to reproduce the optimized bulk value of 2.24 Å. In view of further calculations, we checked the bulklike behavior of tungsten in the presence of Fe layers. We revealed that for 3 ML Fe/W(110) the seven-layer tungsten slab is not thick enough. In this case, one has to take at least nine W layers. Thus, the slabs containing 9 (Fe/7W/Fe), 11 (2Fe/7W/2Fe), and 15 (3Fe/9W/3Fe) atomic layers were taken into consideration. In all three cases a ferromagnetic alignment within the Fe layers was assumed as it was identified as the crucial element in stabilizing the Fe monolayer on W(110) [18]. To minimize artificial interaction between periodic slab images, a 14-Å-thick vacuum region was included in all models. (2×2) supercells with 72 or 88 atoms were used. Eight and six valence electrons for each iron

TABLE I. Interlayer spacings of the best-fit LEED structure of 1 ML Fe/W(110) and 2 ML Fe/W(110) and the DFT optimized structure of 1 ML Fe/W(110), 2 ML Fe/W(110), and 3 ML Fe/W(110). d_{ij} is the interlayer separation between layers i and j with $i = 1$ being the topmost layer. The two-dimensional (2D) cell vectors $\vec{a}$ and $\vec{b}$ give the 2D periodicity of the surface and bulk, while the three-dimensional (3D) repeat vector repeats the bulk layer to form the bulk structure.

Interlayer spacings (Å)				
LEED		DFT		
1 ML Fe/W(110)	2 ML Fe/W(110)	1 ML Fe/7W(110)	2 ML Fe/7W(110)	3 ML Fe/9W(110)
				$d_{12} = 1.76$
	$d_{12} = 1.86 \pm 0.05$		$d_{12} = 1.73$	$d_{23} = 1.85$
$d_{12} = 2.00 \pm 0.02$	$d_{23} = 2.00 \pm 0.06$	$d_{12} = 1.94$	$d_{23} = 2.02$	$d_{34} = 2.00$
$d_{23} = 2.24 \pm 0.03$	$d_{34} = 2.26 \pm 0.07$	$d_{23} = 2.25$	$d_{34} = 2.23$	$d_{45} = 2.23$
$d_{34} = 2.23 \pm 0.04$	$d_{45} = 2.23 \pm 0.07$	$d_{34} = 2.24$	$d_{45} = 2.24$	$d_{56} = 2.24$
$R_p = 0.14 \pm 0.03$	$R_p = 0.16 \pm 0.05$			
	x (Å)	y (Å)	z (Å)	
$\vec{a}$	2.24	1.58		
$\vec{b}$	2.24	-1.58		
Bulk 3D repeat vector	2.24	0.00	2.24	

TABLE II. Layer-resolved magnetic moments of the DFT optimized structure of 1 ML Fe/W(110), 2 ML Fe/W(110), and 3 ML Fe/W(110). Values start from the top film layer.

Magnetic moments (μ_B)		
1 ML Fe/7W(110)	2 ML Fe/7W(110)	3 ML Fe/9W(110)
		2.850
	2.856	2.577
2.469	2.251	2.246

and tungsten atom, respectively, were represented by plane waves with an energy cutoff $E_{\text{cut}} = 390$ eV. Wave functions in the core region were evaluated using the full-potential projector augmented-wave method [41]. The summation in the reciprocal space was performed using the (4×4) $\vec{k}$ grid with four irreducible points, generated with the Monkhorst-Pack scheme [42]. In all calculations the electronic self-consistency criterion has been set to 10^{-7} eV/Å, whereas the ionic relaxations were assumed to be converged when the residual forces on the atoms were below 10^{-4} eV/Å.

1. Surface relaxation

In Table I, we put together all interlayer spacing values obtained from the structural optimization, which allows comparison to the LEED results for the 1 ML Fe/W(110) and 2 ML Fe/W(110) systems. The DFT optimized interlayer spacings show the same trend as those derived from LEED, although the first layer contractions tend to be larger for the former. This is especially evident for the 2 ML Fe/W(110) case, for which the d_{12} contraction is 6.8% larger for DFT. It is worth mentioning here that DFT calculations represent ground state at $T = 0$ and one has to be careful while comparing directly to experimental results. In view of the stability problems discussed below, we also performed the structural optimization for the 3 ML Fe/W(110) system assuming a pseudomorphic phase. The optimized interlayer distances are also listed in Table I.

2. Magnetic moments

In Table II we present the layer-resolved calculated magnetic moments for the three Fe coverages considered. In all cases, we obtain an enhancement with respect to the bulk Fe magnetic moment, which is measured to be $2.2\mu_B$ [43]. The magnetic-moment enhancement is particularly strong in the surface Fe layer of the 2 ML Fe/W(110) system, $2.86\mu_B$, which is in an excellent agreement with previous calculations [34,44,45] and recent experimental results where magnetic moments of 2.90 and $2.25\mu_B$ were estimated for the first and second Fe layers, respectively [16]. Our results for the 3 ML Fe/W(110) system also show a large enhancement of the Fe surface magnetic moment, $2.85\mu_B$, which gradually decreases to the bulk value for deeper layers, in agreement with the theoretical [46] and experimental [7,47] data reported in the literature.

3. Phonon density of states

We analyze the lattice dynamics of the Fe films using the direct method [48], implemented in the PHONON software [22]. The complete set of Hellmann-Feynman forces was obtained by performing small atomic displacements of nonequivalent atoms from their equilibrium positions. Using symmetry elements of the C_{mmm} space group, the force constants were derived, the dynamical matrix was constructed, and next, the phonon frequencies were determined for selected k points in the Brillouin zone (BZ). Finally, phonon dispersion relations were calculated along high symmetry directions of the BZ. Following the notation of Allen *et al.* [49], all high-symmetry points of the 2D BZ are labeled by barred letters. The exact frequencies were calculated at $\bar{\Gamma} = (0,0)$, $\bar{H} = (3/8,3/8)$, $\bar{N} = (1/2,1/2)$, and $\bar{S} = (0,1/2)$ points, in $2\pi/a_i$ units, where a_i is the appropriate lattice constant of the rectangular surface unit cell. First of all, we inspected the phonon dispersion curves for middle tungsten layers in all considered samples. The correct bulklike spectra have been obtained [see Fig. 5(a)]. Next, we performed the calculations for the Fe/7W/Fe nine-layer slab. All phonon frequencies are found to be positive (real), without soft-mode behavior, indicating structural stability of the system. This picture is in agreement with the phonon calculations presented and discussed in detail in Ref. [18].

In Fig. 4 we plot the phonon dispersion curves for the 2 ML Fe/W(110) system, resolving them for the surface (a) and

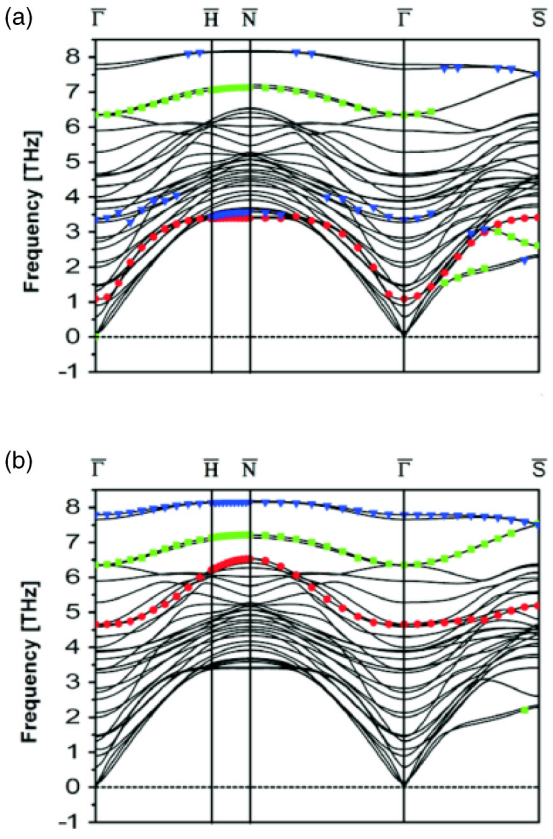

FIG. 4. The calculated phonon dispersion curves for the 2Fe/7W/2Fe 11-layer slab, (a) for the surface Fe layer and (b) for the subsurface Fe layer. Squares (green) and circles (red) denote the highest intensity vibration modes with polarization along the in-plane [001] and [1$\bar{1}$0] directions, respectively. The Rayleigh wave mode, with [110] out-of-plane polarization is marked by triangles (blue).

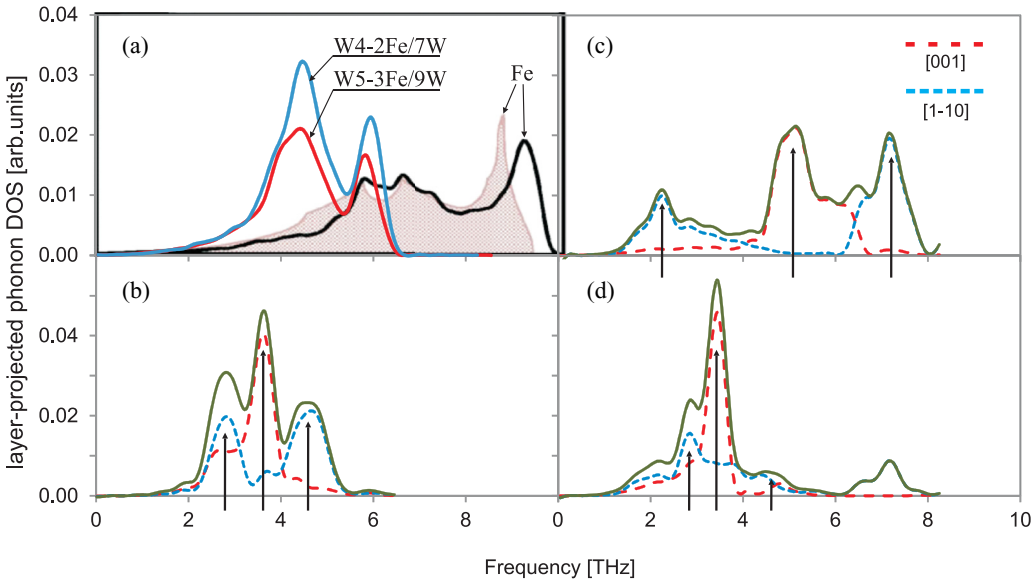

FIG. 5. In-plane phonon DOSs for tungsten and iron bulk [panel (a)]. In-plane (solid lines) phonon DOSs for Fe layers in the 1Fe/7W/1Fe system [panel (b)] and the 2Fe/7W/2Fe system [panels (c) and (d)]. Dotted lines in each panel show the modes with polarization along the in-plane [001] and [1$\bar{1}$0] directions. Arrows indicate the position of main features in the spectra. The iron calculated and experimental phonon DOSs (filled contour) are reproduced from Ref. [50], while the tungsten phonon DOSs are calculated for middle W layers in slabs with 7 and 9 tungsten MLs.

subsurface (b) Fe layers. Squares (green) and circles (red) denote the highest intensity surface vibration modes with polarization along the in-plane [001] and [1$\bar{1}$0] directions, respectively. The Rayleigh wave mode, with [110] out-of-plane polarization is marked by triangles (blue). Any of the surface vibration modes are unstable although the structure of the dispersion relations is quite different from the case of 1 ML Fe/W(110). The Rayleigh wave at the surface layer covers a frequency range partially compatible with that calculated [50] and measured [51] for the semi-infinite Fe(110) system. However, in this case it is not well separated from other phonons. There are some in-plane phonon modes at high frequencies that overlap with the Rayleigh wave. Its frequencies are particularly close to the mode with polarization along the [1$\bar{1}$0] direction. The presence of the interface between Fe and W, materials with different vibrational properties [see Fig. 5(a)] introduces boundary conditions that profoundly affect the vibrational spectrum. This effect manifests itself in mixing of longitudinal and transversal phonon modes. It can be analyzed in more detail by looking at the phonon density of states (DOS) presented layer by layer in Fig. 5 for two systems with 1 and 2 ML Fe/W(110). In each panel we display the total in-plane (solid lines) components, while in panels (b)–(d) the components along [001] and [1$\bar{1}$0] directions (dotted lines) are shown in addition.

Characteristic features of surface phonon spectra for both systems [Figs. 5(b) and 5(d)], namely, the rather low phonon frequencies and the positions of main maxima, are almost unchanged. The spectral weight is different and the main maximum is slightly shifted to lower energy (by ∼5%). However, in the case of the 2 ML Fe/W(110) system a new peak appears at ∼7.15 THz which we explain by the change of the nearest neighbors type from W to Fe atoms. We emphasize that the total phonon DOS for this last mode is much larger than the total phonon DOS of perpendicular vibrations in the considered frequencies range. This suggests that the system can be very close to stability limits and that any additional strain could cause the destabilization of the system and a surface reconstruction along the [1$\bar{1}$0] direction. The subsurface phonon states distribution [Fig. 5(c)] contains both the surface and bulk features. The main surfacelike peak is considerably reduced and shifted towards the lower frequencies. In contrast, the bulklike peak at ∼7.15 THz is substantially enlarged, and a new maximum appears at ∼5.15 THz. It seems to be an interplay between the phonon DOS of the bulk bcc tungsten and iron [see Fig. 5(a)] with the softening due to the surface region, i.e., diminished interlayer distances (see Table I). In the subsurface layer the frequencies of Rayleigh wave increase significantly due to the small mass of the Fe atoms with respect to the neighboring W atoms and the strong reduction of the Fe-W distance (see Table I). The same behavior can be observed in the case of 1 ML but for the 2 ML system the Rayleigh wave has higher frequencies. Moreover, all modes are peeled off the top of the slab band [49]. A change in the interaction between atoms leads to a stiffening of the lattice vibrations and surprisingly stabilizes the 2 ML Fe/W(110) system.

Next we check the stability of the 3 ML Fe/W(110) system. The phonon density of states is presented layer by layer in Fig. 6. First of all, we did not observe any soft modes for this system so the clear conclusion that it is unstable cannot be drawn. However, one has to remember that the dynamical destabilization by dislocations has been observed in our experiment in contrast to the 2 ML Fe/W(110) system. In such confusing situation, we should think over how to correctly interpret the theoretical results without rash conclusions. Let us have a closer look at the phonon density of states (PDOS). One can see that the shape of the PDOS for the Fe layer at the interface [Fig. 6(a)] is quite different from that in

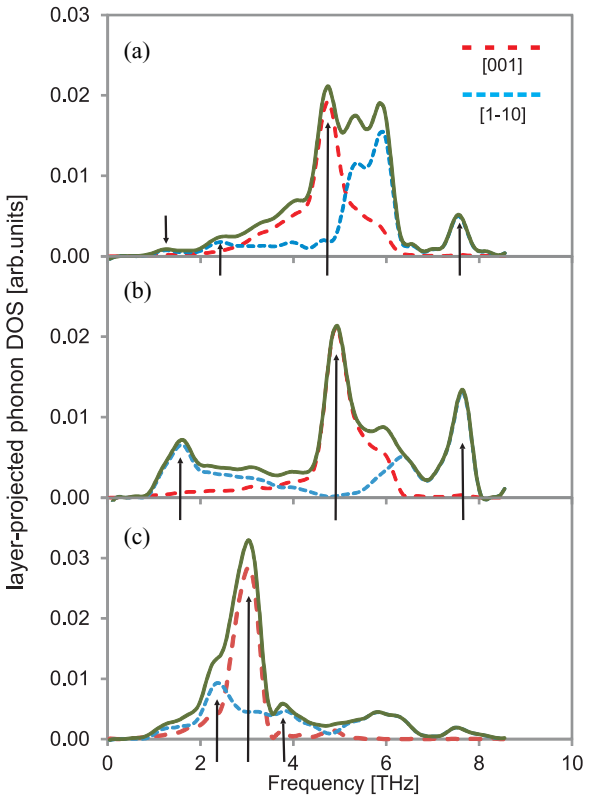

FIG. 6. In-plane (solid lines) phonon DOSs for Fe surface [panel (c)], subsurface [panel (b)], and interface [panel (a)] Fe layers in the 3Fe/9W/3Fe system. Dotted lines in each panel show the modes with polarization along the in-plane [001] and [1$\bar{1}$0] directions. Arrows indicate the position of main features in the spectra.

the 2 ML Fe/W(110) system [Fig. 5(c)]. The spectrum is narrowed and main features are comprised between 4 and 7 THz frequency range, which is characteristic for vibrations in tungsten. In addition, two short peaks can be recognized in the low frequency region and one in the frequency region characteristic for vibrations in iron. In contrast, the PDOS for the subsurface Fe layer [Fig. 6(b)] contains both the surface and bulk structures. The lowest frequency peak is located below 2 THz showing softening of which the first sign can be seen already in the phonon spectrum for Fe at the interface. The rest of the spectrum is shifted towards the higher frequencies specific rather for iron than for tungsten. It seems like a strong competition between vibrations specific for tungsten and iron and destabilization can be expected, particularly that rather big softening is present in the spectrum for the surface Fe layer [compare Figs. 5(b), 5(d), and 6(c)]. Although, looking at the results of phonon calculations, one cannot say unmistakably that three epitaxial iron monolayers are not stable at the W(110) surface, we believe that all symptoms described above lead directly to the conclusion that such system easily destabilizes in contrast to the 2 ML Fe/W(110).

IV. SUMMARY AND CONCLUSIONS

In this work we present an experimental and theoretical study for mono- and bilayer Fe films on a W(110) substrate. We used LEEM to select conditions where 1 and 2 ML films grow layer by layer. For these growth conditions, both 1 and 2 ML Fe are pseudomorphic with the substrate, with no satellite spots in the LEED patterns. Thus, the films of micrometer size are flat. The LEED-$I(V)$ data was fitted to multiple scattering calculations, providing the spacings between the topmost W layer and between any Fe layers. The interplanar spacings of both 1 and 2 ML films are strongly reduced compared to the bulk Fe reference value. It is worthwhile to note that the "bulk" (110) interlayer spacing for Fe film as thick as 4 nm on W(110) still exhibits the reduction by 1% with respect to 2.027 Å characteristic for massive Fe [11]. To better understand the origin of such interplanar spacings and the stability of the pseudomorphic films, we performed first-principles calculations of the structure, the phonon excitation spectra, and the magnetic moments for these two systems and for a pseudomorphic Fe trilayer on W(110). After very careful analyses of phonon dispersion curves and phonon density of states we could conclude that the Fe bilayer is stable but close to the stability limit, while the Fe trilayer shows some symptoms of destabilizing behavior due to the phonon surface modes softening along the [1$\bar{1}$0] direction. It is worth to underline the specific role played by the particular monolayers in each system in the stabilization/destabilization process. For 1 ML Fe/W(110) the in-plane phonon density of states for the surface Fe layer mimic quite well the vibrations of the tungsten (110) surface without any modes characteristic for the iron (110) surface. For the 2 ML Fe/W(110) system, the structure of surface PDOS is almost unchanged, while the Fe layer at the interface exhibits a mixture of tungsten- and ironlike modes with stiffening of the lattice vibrations which seems to stabilize the system. Finally, for 3 ML Fe/W(110), the stabilization role is played by the subsurface Fe layer while two other layers show highly destabilizing behavior, and at the same time softening can be observed in all three Fe layers. However, there is no clear evidence for instability of this system and one cannot exclude a chance to prepare a sample with pseudomorphic 3 ML of Fe on W(110). But, of course we have to remember that calculations are made for a model system.

Our results for the 2 ML Fe/W(110) system do not confirm the formation of periodical misfit dislocations in the second Fe monolayer [5,6], which would lead to the dynamical destabilization and destruction of the pseudomorphic character of this system. The development of misfit dislocations in the early stages of growth can then be associated with the preparation conditions rather than with the system's general properties. We observed significantly relaxed interlayer spacing in the near-surface regions of all the Fe/W(110) systems we examined by experiment and theory. This finding agrees well with predictions for pseudomorphic growth when the adsorbate and substrate have significant lattice mismatch [38].

The magnetic properties of nanoscale materials are currently of considerable scientific and technological interest. In this context, we calculated the magnetic moments for individual Fe layers in the 1 ML Fe/W(110), 2 ML Fe/W(110), and 3 ML Fe/W(110) systems. In all cases, the Fe magnetic moment is enhanced relative to the bulk value. It would be interesting to extend the present calculations to the thermodynamic approach that can shed some light on the film magnetic structure in the layer-resolved mode [52].

ACKNOWLEDGMENTS

This work was financially supported by the Polish Ministry of Science and Higher Education in the frame of Grant No. N N202 259539 and partially by the Spanish Ministry of Innovation and Science under Contracts No. MAT2010-18432 and No. MAT2012-38045-C04-01, and by the Office of Basic Energy Sciences, Division of Materials and Engineering Sciences, U.S. Department of Energy under Contract No. DE-AC04-94AL85000. Parts of the numerical calculations reported in this work have been performed at the Interdisciplinary Center for Mathematical and Computational Modeling (ICM) of the University of Warsaw within Grant No. G53-11.

[1] J. W. M. Frenken, J. F. van der Veen, and G. Allan, Phys. Rev. Lett. **51**, 1876 (1983).

[2] W. T. Lee, L. Ford, P. Blowers, H. L. Nigg, and R. I. Masel, Surf. Sci. **416**, 141 (1998).

[3] Jun-Hyung Cho and M. Scheffler, Phys. Rev. Lett. **78**, 1299 (1997).

[4] M. Calatayud and C. Minot, Surf. Sci. **552**, 169 (2004).

[5] U. Gradmann and G. Waller, Surf. Sci. **116**, 539 (1982).

[6] H. Bethge, D. Heuer, Ch. Jensen, K. Reshöft, and U. Köhler, Surf. Sci. **331-333**, 878 (1995).

[7] J. Korecki and U. Gradmann, Phys. Rev. Lett. **55**, 2491 (1985).

[8] H. J. Elmers, J. Hauschild, H. Fritzsche, G. Liu, U. Gradmann, and U. Köhler, Phys. Rev. Lett. **75**, 2031 (1995).

[9] A. Kubetzka, O. Pietzsch, M. Bode, and R. Wiesendanger, Phys. Rev. B **63**, 140407 (2001).

[10] H. L. Meyerheim, D. Sander, R. Popescu, J. Kirschner, P. Steadman, and S. Ferrer, Phys. Rev. B **64**, 045414 (2001).

[11] M. Rybicki, I. Zasada, K. Freindl, N. Spiridis, and J. Korecki, Appl. Surf. Sci. **286**, 66 (2013).

[12] R. Popescu, H. L. Meyerheim, D. Sander, J. Kirschner, P. Steadman, O. Robach, and S. Ferrer, Phys. Rev. B **68**, 155421 (2003).

[13] B. Santos, J. M. Puerta, J. I. Cerda, R. Stumpf, K. von Bergmann, R. Wiesendanger, M. Bode, K. F. McCarty, and J. de la Figuera, New J. Phys. **10**, 013005 (2008).

[14] Y. Gauthier, R. Baudoing, Y. Joly, C. Gaubert, and J. Rundgren, J. Phys. C **17**, 4547 (1984).

[15] F. El Gabaly, S. Gallego, C. Muñoz, L. Szunyogh, P. Weinberger, C. Klein, A. K. Schmid, K. F. McCarty, and J. de la Figuera, Phys. Rev. Lett. **96**, 147202 (2006).

[16] M. Ślęzak, T. Ślęzak, K. Freindl, W. Karaś, N. Spiridis, M. Zając, A. I. Chumakov, S. Stankov, R. Rüffer, and J. Korecki, Phys. Rev. B **87**, 134411 (2013).

[17] T. Dürkop, H. J. Elmers, and U. Gradmann, J. Magn. Magn. Mater. **172**, L1 (1997).

[18] J. Łażewski, P. Piekarz, A. M. Oleś, J. Korecki, and K. Parlinski, Phys. Rev. B **76**, 205427 (2007).

[19] M. S. Altman, J. Phys.: Condens. Matter **22**, 084017 (2010).

[20] K. F. McCarty and J. de la Figuera, *Surface Science Techniques* (Springer-Verlag, Berlin Heidelberg, 2013), Vol. 51, p. 531.

[21] R. Heid and K.-P. Bohnen, Phys. Rep. **387**, 151 (2003).

[22] K. Parliński, PHONON software, Cracow, 2007.

[23] J. B. Pendry, J. Phys. C **13**, 937 (1980).

[24] C. Jensen, K. Reshöft, and U. Köhler, Appl. Phys. A **62**, 217 (1996).

[25] M. Bode, K. von Bergmann, O. Pietzsch, A. Kubetzka, and R. Wiesendanger, J. Magn. Magn. Mater. **304**, 1 (2006).

[26] J. de la Figuera, K. A. K. Schmid, K. Pohl, N. C. Bartelt, C. B. Carter, and R. Q. Hwang, Mater. Sci. Forum **426-432**, 3421 (2003).

[27] F. El Gabaly, J. M. Puerta, C. Klein, A. Saa, A. K. Schmid, K. F. McCarty, J. I. Cerda, and J. de la Figuera, New J. Phys. **9**, 80 (2007).

[28] A. K. Schmid, N. C. Bartelt, J. C. Hamilton, C. B. Carter, and R. Q. Hwang, Phys. Rev. Lett. **78**, 3507 (1997).

[29] J. de la Figuera, K. Pohl, O. R. de la Fuente, A. K. Schmid, N. C. Bartelt, C. B. Carter, and R. Q. Hwang, Phys. Rev. Lett. **86**, 3819 (2001).

[30] J. de la Figuera (private communication).

[31] H. Huang, S. Y. Tong, W. E. Packard, and M. B. Webb, Phys. Lett. A **130**, 166 (1988).

[32] A. Baraldi, J. Cerdá, J. A. Martín-Gago, G. Comelli, S. Lizzit, G. Paolucci, and R. Rosei, Phys. Rev. Lett. **82**, 4874 (1999).

[33] A. Barbieri and M. A. Van Hove (private communication).

[34] S. C. Hong, A. J. Freeman, and C. L. Fu, Phys. Rev. B **38**, 12156 (1988).

[35] M. Albrecht, U. Gradmann, Th. Reinert, and L. Fritsche, Solid State Commun. **78**, 671 (1991).

[36] E. D. Tober, R. X. Ynzunza, F. J. Palomares, Z. Wang, Z. Hussain, M. A. Van Hove, and C. S. Fadley, Phys. Rev. Lett. **79**, 2085 (1997).

[37] X. Qian and W. Hübner, Phys. Rev. B **60**, 16192 (1999).

[38] D. Sander, A. Enders, and J. Kirschner, Europhys. Lett. **45**, 208 (1999).

[39] J. P. Perdew, K. Burke, and M. Ernzerhof, Phys. Rev. Lett. **77**, 3865 (1996); **78**, 1396 (1997).

[40] G. Kresse and J. Furthmüller, Phys. Rev. B **54**, 11169 (1996).

[41] P. E. Blöchl, Phys. Rev. B **50**, 17953 (1994).

[42] H. J. Monkhorst and J. D. Pack, Phys. Rev. B **13**, 5188 (1976).

[43] H. J. Elmers, G. Liu, and U. Gradmann, Phys. Rev. Lett. **63**, 566 (1989).

[44] A. J. Freeman and C. L. Fu, J. Appl. Phys. **61**, 3356 (1987).

[45] I. Galanakis, M. Alouani, and H. Dreysse, Phys. Rev. B **62**, 3923 (2000).

[46] C. L. Fu and A. J. Freeman, J. Magn. Magn. Mater. **69**, L1 (1987).

[47] T. Ślęzak, J. Łażewski, S. Stankov, K. Parlinski, R. Reitinger, M. Rennhofer, R. Rüffer, B. Sepiol, M. Ślęzak, N. Spiridis, M. Zając, A. I. Chumakov, and J. Korecki, Phys. Rev. Lett. **99**, 066103 (2007).

[48] K. Parlinski, Z.-Q. Li, and Y. Kawazoe, Phys. Rev. Lett. **78**, 4063 (1997).

[49] R. E. Allen, G. P. Alldredge, and F. W. de Wette, Phys. Rev. B **4**, 1648 (1971).

[50] J. Łażewski, J. Korecki, and K. Parlinski, Phys. Rev. B **75**, 054303 (2007).

[51] G. Benedek, J. P. Toennies, and G. Zhang, Phys. Rev. Lett. **68**, 2644 (1992).

[52] M. Rybicki and I. Zasada, J. Phys.: Condens. Matter **24**, 386005 (2012).